Numerical Modeling of Waves and Wave Breaking

A Thesis
Presented to
The Division of Mathematics and Natural Sciences
Reed College

In Partial Fulfillment
of the Requirements for the Degree
Bachelor of Arts

Kevin Freymiller

May 2017

Approved for the Division
(Physics)

_____

Joel Franklin

Acknowledgements

To all of the people who helped me make it through my time here at Reed, thank you. I could not have done it without you. Through all the long days and nights I could not be more grateful for all of the support I've received in so many ways. Thanks for being there when I needed it the most.

Parents - Thank you for giving me such a great education all these years, and thanks for all of the support throughout my life. I never would have looked at the world the same way without you. Thanks for believing in me.

Dad - Thank you for teaching me everything you know, and giving me the curiosity and motivation to change the world around me. Thank you for inspiring my love of science, math, and engineering, I never would have ended up in physics without seeing your work. Your contributions to the scientific community are invaluable and inspiring, and have shown me the potential that I have in my own life, and that even without widespread recognition, the work of a single person can change the world.

Friends - Thank you for all the things you've taught me about myself, and for showing me an alternate way of looking and thinking about the world. You've shown me my value to the world, and have inspired me to push through and try my hardest, and have brought me back up when I was down. You believed in my ability to succeed even when no one else did, and without each and every one of you, I would never have made it to this point.

Joel - I can't imagine this process having gone any smoother. Thanks for your support.

Table of Contents

Introduction **1**
0.1 Conservation Laws 1
0.2 Numerical Methods 2

Chapter 1: Finite-Difference **3**
1.1 Equations of Motion 3
1.2 Non-Dimensionalization 5
1.3 Lax-Friedrichs Method 6
1.4 Lax Friedrichs Application 7
1.5 Modified Lax Friedrichs 8
1.6 Results 9
1.6.1 Results for $\alpha = 0$ 9
1.6.2 Results for $\alpha > 0$ 9
1.7 Stability of the modified Lax-Friedrichs Method 10

Chapter 2: Balls and Springs **15**
2.1 Elastic Network Models 16
2.2 Equations 16
2.3 Verlet 18
2.4 Constant k 19
2.5 Changing k by angle 19
2.6 More physical k 21
2.7 Energy measurement 21
2.8 Energy k 22
2.9 Breaking Test 24

Chapter 3: Combination of Methods **27**
3.1 Conversion of Data 27
3.2 Parameters for the Full Simulation 29
3.3 Results 29
3.4 Comparison to Experiments 32

Conclusion **35**

References **37**

List of Figures

1.1 2-dimensional cross section of a gently sloped beach, the scenario used in this chapter. The water has density ρ_0, a surface is defined by $h(x,t)$, and arrows indicate velocity vectors with components v_x and v_z. The vertical component, v_z is defined according to the boundary conditions in Eq. 1.6. The bottom is uniform, with slope α. Water moving near the bottom is forced to flow parallel to it. 4

1.2 The flow of water close to the sloped bottom must move parallel to it, to keep flux through the bottom at 0 [5]. 5

1.3 The discretization used in the Lax-Friedrichs method, with positions separated by Δx on the horizontal axis, and each time step, Δt apart, on the vertical axis. To calculate the value at (x_j, t_{n+1}), the points (x_{j-1}, t_n) and (x_{j+1}, t_n) are needed. 6

1.4 Wave propagation for $\alpha = 0$. The initial gaussian, shown in red at time $s = 0$, creates a left-traveling and right-traveling wave, with waveforms shown at times $s = 0.25$ and $s = 0.5$. 10

1.5 Scatter plot of the position q of the peak height of the right traveling wave as a function of time s. The initial flat section corresponds to the initial Gaussian collapsing before it moves outward. The green fit line is a linear fit of the data from $3.5s$ to $7.5s$ (r=0.9996), a region where the velocity is nearly constant. The non-dimensional velocity was found to be 1.16. 11

1.6 As the wave approaches breaking, the right and left traveling velocities cancel, and the wave appears to sink below the surface. 11

1.7 Starting with the initial Gaussian, the effect of the slope can be seen in the right traveling wave which has a larger height, shown at $s = 7.5$. 12

1.8 Comparison of the stability of η_j^{n+1} in the k_j^{n+1} equation. The calculated solution including η_j^{n+1} is the smooth function, while the modified version substituting η_j^n is the more jagged solution with discontinuities beginning to form. This modification resulted in instability and is shown at 485 steps, just before the discontinuities grow to infinity and the model breaks. 13

2.1 Setup for the ball and spring model. 16

2.2 Basic behavior of a connected spring system with fixed endpoints. The initial Gaussian wave collapses in the center and creates two waves that propagate to the left and right. The wave height decreases and is reversed as it moves past the endpoints, and the wave then propagates the other direction but upside down. The initial height is a solid line, with the dashed lines at later times. 20
2.3 Description of angles used to modify k. This is similar to the curvature of a string adapted from a continuous to discrete system. 20
2.4 Relevant variables used in Eq. 2.11. h is the height of the wave above the ambient water height, h_0, and d is the depth of the water at that point, the distance to the linear sloping bottom. 21
2.5 With the damping term $\gamma = 0$, the loop that initially forms to break the wave increases in size until the wave is only represented by that loop propagating to the right. Each dashed line further to the right represents a later point in time. 22
2.6 Energy for a wave using the update for k in Eq. 2.15, shown in the lower line with the wave above. Energy peaks just behind the peak of the wave, where the springs are the most stretched. But more importantly, a second peak is visible at the leading tip of the wave, which corresponds to a region in which the springs are compressed, and the modified spring constants give that region a boost in energy. 23
2.7 Wave breaking, with initial wave velocity to the right. 25
2.8 Velocity profile given by the methods in Chapter 1 for a collapsing Gaussian, shortly after the simulation begins. The velocity profile for the right and left traveling waves is each close to a Gaussian, so using that as the initial velocity of the ball and spring model is reasonable. 25

3.1 Assuming the initial position of the ball is at the height of the wave for calculation point j, I could assume that the ball in the next time step had moved to any of the other points (or more) shown for a wave moving to the right. If the point were to move directly up, the vertical component of velocity would change significantly between the two models, but if it only moves to the right, it neglects some non-zero vertical component. 28
3.2 The full simulation shown from $s = 0$ to $s = 5$. The Lax-Friedrichs model runs from 0 to 1, and the Verlet model runs from 1 to 5. 30
3.3 Wave at $s = 8$. The leading edge of the wave collapses and forms a loop, at which point the solution is no longer an accurate representation of wave behavior. 31
3.4 Full simulation of the wave. 32

Abstract

In Chapter 1, equations of motion based on the Navier-Stokes equations of mass and momentum continuity were developed in the two-dimensional case, with a linear sloping bottom introduced through the lower bounds of integration, modifying the shallow water equations. These equations were solved using the Lax-Friedrichs method, which was modified to account for the non-conservative nature of the modified shallow water equations. In Chapter 2, a model representing the surface of a water wave was developed using balls and springs. The spring constant was varied according to the height of the wave and the depth of the water.

In Chapter 3, the two methods were combined, constructing a wave near breaking using the Navier-Stokes equations, and then just before breaking, which is not allowed in the Lax-Friedrichs method, passing the data into the ball and spring model to observe the breaking behavior.

Introduction

0.1 Conservation Laws

The motion and disturbance of water behaves classically, so Newton's laws and conservation of mass, momentum and energy can be applied to the case of the one-dimensional wave. In this section, I derive the Navier-Stokes continuity equations, from base principles of conservation of mass and momentum to equations of motion that can be applied to the physical situation of the sloping beach [1]. To develop an equation of motion from conservation of mass, begin with the notion that the flow of mass out of a volume V is equivalent to the flow of mass through its outer surface S.

$$\int_S \vec{J} \cdot d\vec{A} = -\frac{\mathrm{d}}{\mathrm{d}t} \int_V \rho \, dV = -\int_V \frac{\partial \rho}{\partial t} \, dV, \tag{1}$$

where $\vec{J} = \rho\vec{v}$, analogous to current density in electrodynamics, ρ is the constant density of the fluid, and $\vec{v}$ is the velocity vector at a particular point. Note that by the divergence theorem,

$$\int_S \vec{J} \cdot d\vec{A} = \int_V \nabla \cdot \vec{J} \, dV, \tag{2}$$

which allows Eq. 1 to be simplified to

$$\nabla \cdot \vec{J} = -\frac{\partial \rho}{\partial t}, \tag{3}$$

with the integrals over the same variable removed. This can be rewritten component-wise,

$$\frac{\partial \rho}{\partial t} + \frac{\partial}{\partial x_i}(\rho v_i) = 0, \tag{4}$$

written in Einstein notation, where the terms with multiple indices imply a sum of all combinations. This is the Navier-Stokes continuity equation for mass. Similarly, to create a continuity equation for momentum, note that force is equal to the change in momentum over time,

$$\vec{F}_{net} = m\vec{a} = \frac{\mathrm{d}}{\mathrm{d}t}(m\vec{v}), \tag{5}$$

where m is the mass of the volume element. Within a reference volume dV, momentum change can come in two pieces, the change of momentum inside of dV and the flow of momentum through the outer surface, so

$$\frac{\mathrm{d}}{\mathrm{d}t}\left(\int_V \rho\vec{v} dV\right) = \frac{\partial}{\partial t} \int_V \vec{J} \, dV + \int_S \vec{v}(\vec{J} \cdot \vec{n}) \, dA, \tag{6}$$

where $\vec{n}$ is the vector normal to a point dA on the surface S. Again using the divergence theorem,

$$\int_S (\vec{v}\vec{J}) \cdot \vec{n}\, dA = \int_V \nabla \cdot (\vec{v}\vec{J})\, dV. \tag{7}$$

Removing the integrals which are the same on both sides,

$$\vec{F} = \frac{\partial}{\partial t}\left(\vec{J}\right) + (\nabla \cdot \rho\vec{v}\vec{v}). \tag{8}$$

Note that to ensure momentum continuity, all of these terms should add to the change in potential energy. Rewriting component wise and replacing $\vec{J}$ with $\rho\vec{v}$,

$$\frac{\partial}{\partial t}(\rho v_i) + \frac{\partial}{\partial x_j}(\rho v_i v_j) + \frac{\partial u}{\partial x_i} = 0. \tag{9}$$

The term $\frac{\partial u}{\partial x_i}$ is added to account for a change in momentum due to an external potential, which is gravitational potential gh in this case. This is the final continuity equation for conservation of momentum.

0.2 Numerical Methods

The partial differential equations used in this thesis are quite complex and are highly non-linear, and therefore cannot be analytically solved, except in a handful of particular situations. To get a wave to break requires significant complexity, despite the simplifying assumptions made, and integrals need to be solved numerically. A tremendous number of numerical methods are used in physics today, but I was faced with several options in the choice of method. Finite difference methods, used in Chapter 1, solve the equations at specific points based on the behavior in the previous time step, and calculate differences between those times and the adjacent calculation points. In a finite difference model, you might calculate the height of the water at the point $x = 1$. Finite element methods breaks up the simulation into small regions, within which the equations are solved. Here you would calculate that water fills the entirety of a specific region in the grid, based on whether the adjacent regions are also filled with water among other factors. A good introduction to computational methods can be found in Joel Franklin's Computational Methods for Physics [2] and Joel Ferziger's Computational Methods for Fluid Dynamics [1].

The methods used in this thesis are relatively simple, and can run easily on a laptop computer in under a minute. State of the art fluid simulations are significantly more complex, and require hours to days to run on supercomputers. The most popular and realistic method used today is called Smoothed Particle Hydrodynamics [3], which simulates the motion of individual particles, usually numbering several million. For each particle, viscosity, pressure, changes in density, and intermolecular forces are calculated between all of the other particles in close proximity in addition to the motion of the particles, using numerical integration at every time step.

Chapter 1

Finite-Difference

A wave breaking on a beach is an incredibly complex process, and modeling its actual behavior by solving the Navier-Stokes equations directly on a computer could not occur in a reasonable time. Instead, I make some assumptions about the wave behavior and the scene in which they exist so that I can graduate on time. The basic setup is shown in Fig. 1.1, where a wave in two dimensions is defined by the height of the surface and the velocity at every point which will be restricted such that the x-component of velocity, $v_x(x,t)$ is defined at each point in x and constant for all z at a given x and t. The bottom is a line with a small linear slope of α. The water is assumed incompressible, so has constant density ρ_0 and zero curl.

1.1 Equations of Motion

In this section I derive the equations of motion from the statement of mass and momentum continuity in Eqs. 4 and 9 through integration in z. This derivation is similar to the shallow water equations, and is adapted from [4]. These equations are valid where water is present, below the surface h and above the bottom αx. While the functions could be defined piecewise, delta and Heaviside-theta functions are used to delineate the regions above and below h (between αx and h), while still keeping the function defined for all z from $-\infty$ to ∞. To accomplish this, the density, ρ takes the form

$$\rho(x,z,t) = \rho_0(\Theta(h(x,t)-z) - \Theta(\alpha x - z)), \tag{1.1}$$

where ρ_0 is the density of water, which is nearly incompressible and is therefore assumed here to be constant. Plugging this in, Eq. 4 becomes

$$\delta(h-z)\frac{\partial h}{\partial t} + v_x\Big(\delta(h-z)\frac{\partial h}{\partial x} - \delta(\alpha x - z)\alpha\Big) + \frac{\partial v_x}{\partial x}\Big(\Theta(h-z) - \Theta(\alpha x - z)\Big) = 0, \tag{1.2}$$

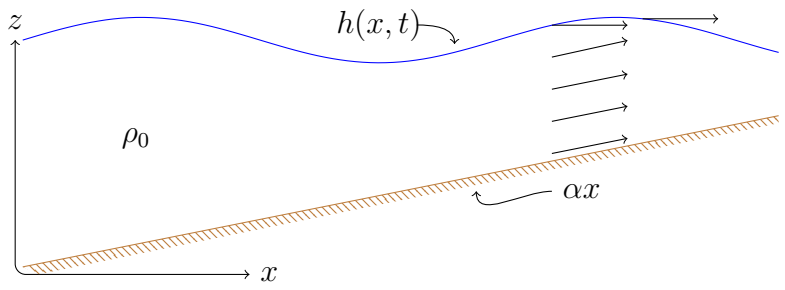

Figure 1.1: 2-dimensional cross section of a gently sloped beach, the scenario used in this chapter. The water has density ρ_0, a surface is defined by $h(x,t)$, and arrows indicate velocity vectors with components v_x and v_z. The vertical component, v_z is defined according to the boundary conditions in Eq. 1.6. The bottom is uniform, with slope α. Water moving near the bottom is forced to flow parallel to it.

for mass conservation, and Eq. 9 becomes

$$\begin{aligned}&\delta(h-z)\frac{\partial h}{\partial t}v_x + \frac{\partial v_x}{\partial x}(\Theta(h-z)-\Theta(\alpha x-z)) + v_x^2(\delta(h-z)\frac{\partial h}{\partial x}-\delta(\alpha x-z)\alpha)\\ &+\frac{\partial}{\partial x}\left(v_x^2\right)(\Theta(h-z)-\Theta(\alpha x-z)) + v_x v_z(-\delta(h-z)+\delta(\alpha x-z))\\ &+\frac{\partial}{\partial z}(v_x v_z)(\Theta(h-z)-\Theta(\alpha x-z)+\frac{1}{\rho_0}\frac{\partial u}{\partial x}=0\end{aligned} \tag{1.3}$$

for momentum continuity. Integrating over all z, the delta functions eliminate the integrals for their associated terms, and the Heaviside-theta functions leave integrals with limits of integration $\alpha x \to h$,

$$\frac{\partial h}{\partial t} + v_x\frac{\partial h}{\partial x} - \alpha v_x + \int_{\alpha x}^{h} h\frac{\partial v_x}{\partial x}dz = 0 \tag{1.4}$$

and

$$v_x\frac{\partial h}{\partial t} + v_x^2\left(\frac{\partial h}{\partial x}-\alpha\right) + v_x v_z|_{\alpha x} + \int_{\alpha x}^{h}\left(\frac{\partial v_x}{\partial t}+\frac{\partial}{\partial x}\left(v_x^2\right)+v_x\frac{\partial v_z}{\partial z}+v_z\frac{\partial v_x}{\partial z}+\frac{1}{\rho_0}\frac{\partial u}{\partial x}\right)dz \tag{1.5}$$

Applying boundary conditions on the velocity, assume

$$\begin{aligned}v_z(z=h)&=0\\ v_z(z=\alpha x)&=\alpha v_x.\end{aligned} \tag{1.6}$$

This constrains the water to remain below the surface h, and flux through the surface will stay at 0. Likewise, in order for water to not flow through the bottom, it must move parallel to the surface, as shown in Fig. 1.2 [5]. This eliminates some terms in the integrals, giving

$$\frac{\partial h}{\partial t} + v_x\frac{\partial h}{\partial x} + \frac{\partial v_x}{\partial x}(h-\alpha x) - \alpha v_x = 0, \tag{1.7}$$

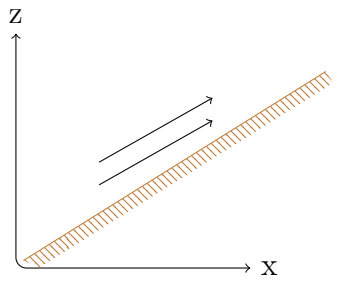

Figure 1.2: The flow of water close to the sloped bottom must move parallel to it, to keep flux through the bottom at 0 [5].

which is the complete shallow water equation for conservation of mass. For momentum continuity we have,

$$\frac{\partial}{\partial t}(hv_x) - \alpha x\frac{\partial v_x}{\partial t} + v_x^2\left(\frac{\partial h}{\partial x} - \alpha\right) + (h - \alpha x)\frac{\partial}{\partial x}\left(v_x^2\right) + gh\frac{\partial h}{\partial x} = 0, \tag{1.8}$$

the complete shallow water equation for conservation of momentum. This can be simplified into roughly conservative form, combining multiple time and position derivatives into a single derivative for both time and position with a non-conservative offset term. Performing the re-groupings gives,

$$\frac{\partial h}{\partial t} + v_x\frac{\partial h}{\partial x} + \frac{\partial v_x}{\partial x}(h - \alpha x) - \alpha v_x = 0 \tag{1.9}$$

and

$$\frac{\partial}{\partial t}(v_x h - v_x\alpha x) + \frac{\partial}{\partial x}(hv_x^2 + \frac{1}{2}gh^2) - \frac{\partial v_x}{\partial x}2v_x\alpha x - v_x^2\alpha = 0. \tag{1.10}$$

as the modified shallow water equations for the sloped bottom problem in their complete form.

1.2 Non-Dimensionalization

To move forward with the numerical modelling, Eqns. 1.9 and 1.10 must be changed into a dimensionless form. To do this, h, v, x and t are replaced with $h = h_0\eta$, $x = x_0 q$, and $t = t_0 s$, where the zero-subscripted terms carry their respective units. To neaten the notation, velocity v is substituted using $J = vh$, or $v = {}^{J}/_{h}$, and is made dimensionless by $J = v_0 h_0 k$. This gives

$$\frac{1}{t_0}\frac{\partial h_0\eta}{\partial s} + \frac{1}{x_0}\frac{\partial}{\partial q}\left(v_0 h_0 k - \frac{v_0 h_0 k}{h_0\eta}\alpha x_0 q\right) = 0 \tag{1.11}$$

and

$$\begin{aligned}&\frac{1}{t_0}\frac{\partial}{\partial s}\left(h_0 v_0 k + \frac{h_0 v_0 k\alpha x_0 q}{h_0\eta}\right) + \frac{1}{x_0}\frac{\partial}{\partial q}\left(\frac{h_0^2 v_0^2 k^2}{h_0^2\eta^2} + \frac{1}{2}gh_0^2\eta^2 - \frac{1}{2}\frac{h_0 v_0 k}{h_0\eta}\alpha x_0 q\right)\\ &+ \frac{1}{x_0}\frac{\partial}{\partial q}\left(\frac{v_0 h_0 k}{h_0\eta}\right)\frac{v_0 h_0 k}{h_0\eta}2\alpha x_0 q - \alpha\left(\frac{v_0 h_0 k}{h_0\eta}\right)^2 = 0.\end{aligned} \tag{1.12}$$

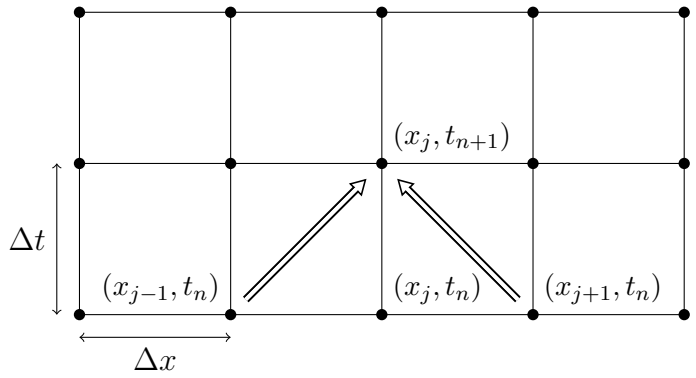

Figure 1.3: The discretization used in the Lax-Friedrichs method, with positions separated by Δx on the horizontal axis, and each time step, Δt apart, on the vertical axis. To calculate the value at (x_j, t_{n+1}), the points (x_{j-1}, t_n) and (x_{j+1}, t_n) are needed.

To eliminate some constants, let ${}^{h_0}/_{t_0} = v_0$, $x_0 = h_0$ and $t_0^2 = {}^{h_0}/_{g}$. With these, the equations simplify to

$$\frac{\partial \eta}{\partial s} + \frac{\partial}{\partial q}\left(k\left(1 - \frac{\alpha q}{\eta}\right)\right) = 0 \tag{1.13}$$

and

$$\frac{\partial}{\partial s}\left(k\left(1 + \frac{\alpha q}{\eta}\right)\right) + \frac{\partial}{\partial q}\left(\frac{k^2}{\eta} + \frac{1}{2}\eta^2\right) - \frac{\partial}{\partial q}\left(\frac{k}{\eta}\right)\frac{2\alpha q k}{\eta} - \alpha\left(\frac{k}{\eta}\right)^2 = 0. \tag{1.14}$$

This is the complete form for the shallow water equations to which the Lax-Friedrichs method can be applied, as described in the following section.

1.3 Lax-Friedrichs Method

Lax-Friedrichs is a numerical method for solving partial differential equations of the form

$$\frac{\partial h(x,t)}{\partial t} + \frac{\partial}{\partial x}(v(x,t) \cdot h(x,t)) = 0. \tag{1.15}$$

where h is, for example, the height of a wave, and v is the velocity for points on the wave, given initial conditions $h(x,0) = f(x)$, as well as any relevant boundary conditions. The method uses discretized space and time. We'll take a grid with constant spacing Δx and Δt, depicted in Fig. 1.3, with

$$\begin{aligned} x_j &= j\Delta x \\ t_n &= n\Delta t. \end{aligned} \tag{1.16}$$

To neaten the notation, let

$$h_j^n \equiv h(x_j, t_n). \tag{1.17}$$

Time derivatives will be one-sided, meaning that time derivatives only consider t_n when solving for t_{n+1}, while spatial derivatives will be centered, depending on x_{j-1} and x_{j+1}, ignoring x_j. To reconstruct derivatives within this grid, consider the Taylor approximation of h at time $n+1$,

$$\begin{aligned} h_j^{n+1} &= h_j^n + \frac{\partial(h_j^n)}{\partial t}\Delta t + \cdots \\ \frac{\partial(h_j^n)}{\partial t} &\approx \frac{h_j^{n+1} - h_j^n}{\Delta t}. \end{aligned} \tag{1.18}$$

Spatial derivatives here are of the same basic form, but over a distance of $2\Delta x$,

$$\frac{\partial(h_j^n)}{\partial x} \approx \frac{h_{j+1}^n - h_{j-1}^n}{2\Delta x}. \tag{1.19}$$

This method can propagate the initial wave conditions forward in time for all points x_j in the grid. Applying Eqns. 1.18 and 1.19 to the PDE in Eq. 1.15,

$$h_j^{n+1} = h_j^n - \frac{\Delta t}{2\Delta x}(h_{j+1}^n\, v_{j+1}^n - h_{j-1}^n\, v_{j-1}^n). \tag{1.20}$$

The final step in the Lax-Friedrichs method is to replace the single h_j^n term associated with the time derivative with the average of adjacent points, which serves to dampen the effects of any large deviations of a single point. With this substitution, the Lax-Friedrichs method is complete for solving conservative equations.

$$h_j^{n+1} = \frac{1}{2}(h_{j-1}^n + h_{j+1}^n) - \frac{\Delta t}{2\Delta x}(h_{j+1}^n\, v_{j+1}^n - h_{j-1}^n\, v_{j-1}^n) \tag{1.21}$$

To further ensure stability, Δx and Δt must be appropriately chosen, such that

$$|v|\Delta t \leq \Delta x \tag{1.22}$$

at every time step [2].

1.4 Lax Friedrichs Application

The equation of motion derived from mass continuity, Eq. 1.13, is conservative, so no modification of the method is required. Replacing the derivatives,

$$\frac{\eta_j^{n+1} - \eta_j^n}{\Delta s} + \frac{1}{2\Delta q}\left[k_{j+1}^n\left(1 - \frac{\alpha(j+1)\Delta q}{\eta_{j+1}^n}\right) - k_{j-1}^n\left(1 - \frac{\alpha(j-1)\Delta q}{\eta_{j-1}^n}\right)\right] = 0. \tag{1.23}$$

Solving for η_j^{n+1},

$$\eta_j^{n+1} = \eta_j^n - \frac{\Delta s}{2\Delta q}\left(k_{j+1}^n\frac{1-\alpha(j+1)\Delta q}{\eta_{j+1}^n} - k_{j-1}^n\frac{1-\alpha(j-1)\Delta q}{\eta_{j-1}^n}\right). \tag{1.24}$$

To complete the equation, apply the averaging condition to η_j^n,

$$\eta_j^{n+1} = \frac{1}{2}(\eta_{j+1}^n + \eta_{j-1}^n) - \frac{\Delta s}{2\Delta q}\left(k_{j+1}^n\frac{1-\alpha(j+1)\Delta q}{\eta_{j+1}^n} - k_{j-1}^n\frac{1-\alpha(j-1)\Delta q}{\eta_{j-1}^n}\right). \tag{1.25}$$

1.5 Modified Lax Friedrichs

Lax-Friedrichs does not work as-is for this problem, since only Eq. 1.13 is in conservative form. Despite this, note that Eq. 1.14, can be written in a nearly conservative form, with some extra terms. In this section, I proceed with applying the method as if it were conservative. Substituting the derivatives in Eq. 1.14 with the usual Lax-Friedrichs approximations,

$$\frac{1}{\Delta s}\left[k_j^{n+1}\left(1+\frac{\alpha j\Delta q}{\eta_j^{n+1}}\right)-k_j^n\left(1+\frac{\alpha j\Delta q}{\eta_j^n}\right)\right]+\frac{1}{2\Delta q}\left[\frac{k_{j+1}^n}{\eta_{j+1}^n}+\frac{1}{2}(\eta_{j+1}^n)^2-\frac{k_{j-1}^n}{\eta_{j-1}^n}+\frac{1}{2}(\eta_{j-1}^n)^2\right]$$
$$-\frac{1}{2\Delta q}\left(\frac{k_{j+1}^n}{\eta_{j+1}^n}-\frac{k_{j-1}^n}{\eta_{j-1}^n}\right)\frac{2\alpha j\Delta q k_j^n}{\eta_j^n}-\alpha\left(\frac{k_j^n}{\eta_j^n}\right)^2=0. \tag{1.26}$$

Solving for the desired value, k_j^{n+1}, we have

$$k_j^{n+1}=\frac{1}{\left(1+\frac{\alpha j\Delta q}{\eta_j^{n+1}}\right)}\left\{k_j^n\left(1+\frac{\alpha j\Delta q}{\eta_j^n}\right)+\frac{\Delta s}{2\Delta q}\left[\left(\frac{k_{j+1}^n}{\eta_{j+1}^n}-\frac{k_{j-1}^n}{\eta_{j-1}^n}\right)\frac{2\alpha j\Delta q k_j^n}{\eta_j^n}\right.\right.$$
$$\left.\left.-\left(\frac{k_{j+1}^n}{\eta_{j+1}^n}+\frac{1}{2}(\eta_{j+1}^n)^2-\frac{k_{j-1}^n}{\eta_{j-1}^n}+\frac{1}{2}(\eta_{j-1}^n)^2\right)\right]-\alpha\left(\frac{k_j^n}{\eta_j^n}\right)^2\right\}. \tag{1.27}$$

This equation has a few major differences from the conservative solution in Eq. 1.21. First of all, note that k_j^n occurs in several places. According to the Lax-Friedrichs method, these terms should be replaced with the average of the adjacent values. However, this term occurs in multiple places as a result of the extra part of Eq. 1.14 that prevents it from being conservative. Therefore, in this modified method, I've chosen to modify only the k_j^n term that was associated with the time derivative, the only place k would show up if the equation was in the form for the true Lax-Friedrichs method. Applying the averaging condition, we have

$$k_j^{n+1}=\frac{1}{\left(1+\frac{\alpha j\Delta q}{\eta_j^{n+1}}\right)}\left\{\frac{1}{2}\left(\frac{k_{j+1}^n(1+\alpha(j+1)\Delta q}{\eta_{j+1}^n}+\frac{k_{j-1}^n(1+\alpha(j-1)\Delta q)}{\eta_{j-1}^n}\right)\right.$$
$$-\frac{\Delta s}{2\Delta q}\left[\frac{(k_{j+1}^n)^2}{\eta_{j+1}^n}-\frac{(k_{j-1}^n)^2}{\eta_{j-1}^n}+\frac{1}{2}\big((\eta_{j+1}^n)^2-(\eta_{j-1}^n)^2\big)\right] \tag{1.28}$$
$$\left.+\left(\frac{k_{j+1}^n}{\eta_{j+1}^n}-\frac{k_{j-1}^n}{\eta_{j-1}^n}\right)\frac{2\alpha j\Delta q k_j^n}{\eta_j^n}-\alpha\left(\frac{k_j^n}{\eta_j^n}\right)^2\right\}.$$

The next major difference in this equation is the η_j^{n+1} term. This term results from the time derivative in Eq. 1.14,

$$\frac{\partial}{\partial s}\left(k\left(1+\frac{\alpha q}{\eta}\right)\right), \tag{1.29}$$

resulting in an extra η_j^{n+1}. In the traditional Lax-Friedrichs solution, there is only one term in the time derivative, avoiding this issue. However this is not a problem as there are two separate equations, the update step in the code can simply calculate the update for η first and plug in the answer. An alternative could be to replace η_j^{n+1} with η_j^n, modifying to more closely fit the original Lax-Friedrichs method. The effects of this are explored in Section 1.7.

1.6 Results

1.6.1 Results for $\alpha = 0$

Using the Lax-Friedrichs model with α of zero, the equations simplify to the shallow water equations and can be compared to previous results. With an initial Gaussian curve for η,

$$\eta(q) = e^{\frac{1}{2}(q-\frac{L}{2})^2} + 1, \tag{1.30}$$

where L is the width of the window in which the model runs. Spatial and time discretization, dq and ds, respectively were chosen,

$$\begin{aligned} dq &= \frac{L}{200} \\ ds &= \frac{dq}{10}. \end{aligned} \tag{1.31}$$

The results for this case behave as expected qualitatively. The initial wave falls, and two waves moving at the same speed propagate to the left and right. This case is similar to that of the linearized shallow water equations, with the bottom not explicitly defined. Valid for large scale waves like tsunamis, the linearized form of these equations allows for an approximation of the propagation velocity that is close to experimental results. These linearized equations can actually be solved for v, giving $v \approx \sqrt{gh}$, which corresponds to a dimensionless velocity of 1 [5]. A depth of 1 resulted in a non-dimensional velocity of 1.16, and is the depth used in the rest of the thesis.

1.6.2 Results for $\alpha > 0$

With α set to 0.05, the same input Gaussian was tested. The maximum height of the right traveling wave was above that of the left traveling wave, an expected result since the depth of the water decreases as the wave travels to the right. Initial velocity was similar to the flat case, but as the wave approaches shallow water, it slows down and eventually stops. Since the sloped bottom is implicitly defined in the bounds of the integrals, it is possible for η to be defined below αx, and the resulting output of the equations has v_x equal to 0, which leads to the wave sinking below the surface once it has stopped moving to the right, as shown in Fig 1.6. The wave height depicted below the surface is not a physical result, and that data should be ignored. However, as the

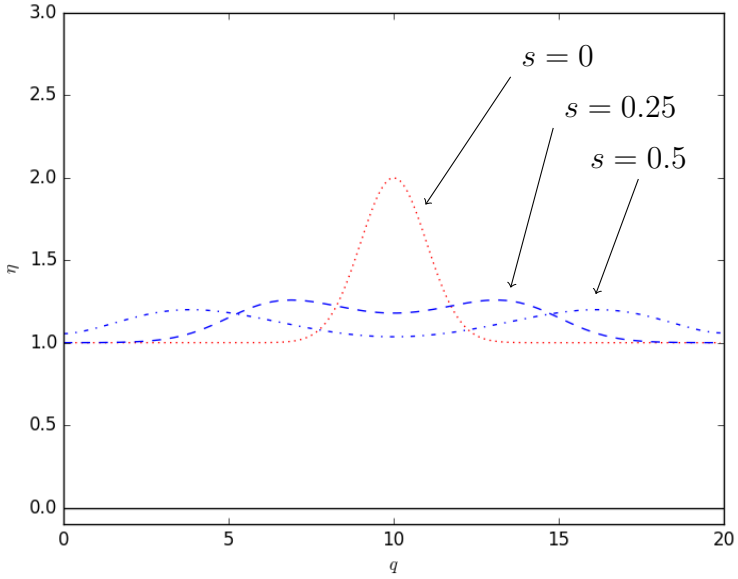

Figure 1.4: Wave propagation for $\alpha = 0$. The initial gaussian, shown in red at time $s = 0$, creates a left-traveling and right-traveling wave, with waveforms shown at times $s = 0.25$ and $s = 0.5$.

wave approaches the bottom as it travels to the right, the leading edge of the wave increases in its steepness, which appears to lead to a breaking situation if the model allowed for such a result. This is not allowed since the velocity is restricted such that water below the wave front cannot pass underneath and to the left while the top of the wave continues moving to the right, since v_x is constant for a given x and t. The near-breaking scenario can be even more clearly seen when initial velocities are added such that the wave is traveling to the right, while the water in front of it is moving to the left, analogous to what can be seen on a beach where the water pushed up the slope of the beach from the previous wave must flow backwards and contributes to the breaking of the following wave.

1.7 Stability of the modified Lax-Friedrichs Method

The modified Lax-Friedrichs method was verified to stay within the same requirements as the usual form, that is,

$$|v|dt \leq dx \tag{1.32}$$

was verified for each point at each time step. This stability requirement says that the distance travelled between time steps is less than the spacing between calculation points. If this is not met, the velocity would be high enough that in one time step it would move beyond one division of space. For example, if a wave is moving at 10 $^{\mathrm{m}}/_{\mathrm{s}}$, with $dt = 1\mathrm{s}$ and $dx = 1\mathrm{m}$, between two time steps, the wave would have

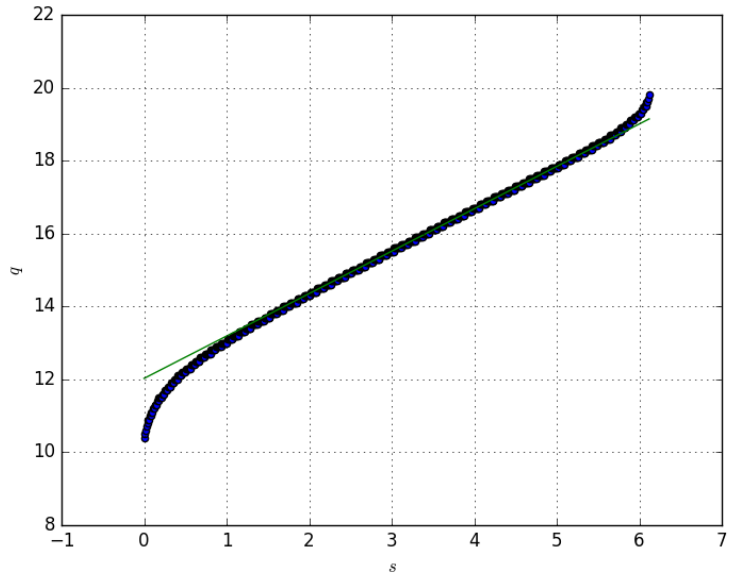

Figure 1.5: Scatter plot of the position q of the peak height of the right traveling wave as a function of time s. The initial flat section corresponds to the initial Gaussian collapsing before it moves outward. The green fit line is a linear fit of the data from $3.5s$ to $7.5s$ (r=0.9996), a region where the velocity is nearly constant. The non-dimensional velocity was found to be 1.16.

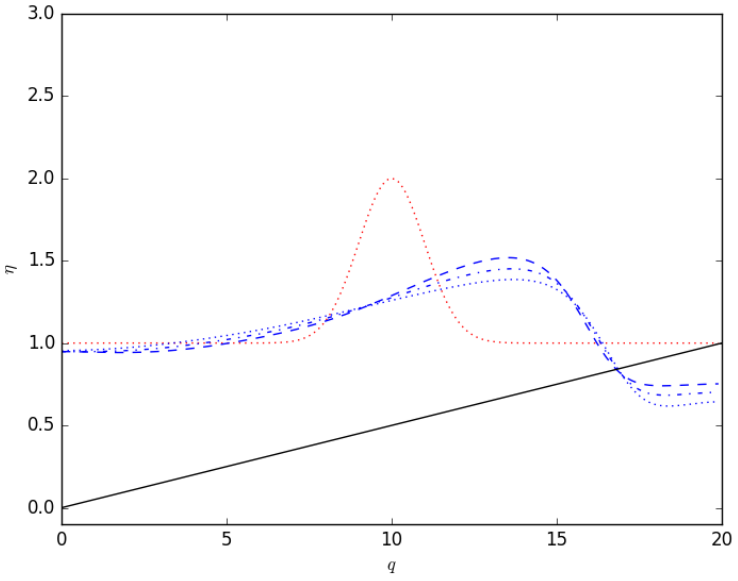

Figure 1.6: As the wave approaches breaking, the right and left traveling velocities cancel, and the wave appears to sink below the surface.

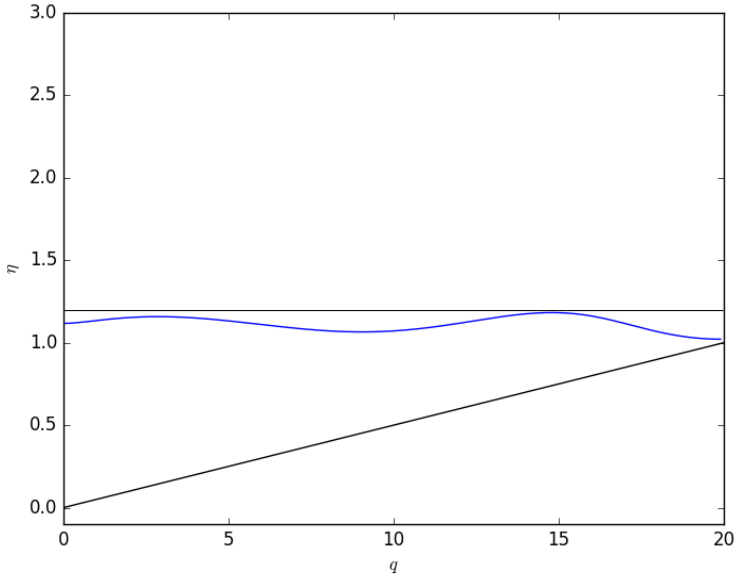

Figure 1.7: Starting with the initial Gaussian, the effect of the slope can be seen in the right traveling wave which has a larger height, shown at $s = 7.5$.

moved across 10 points at which the height is calculated. This solution could be unstable, and some points could quickly diverge, sending the wave height to infinity erroneously. Also given the non-linear behavior of the waves, such a large time step would ignore potentially important evolution in the behavior of the wave, even if the solution appeared to be stable. Since the modified version of the equations results in a η_j^{n+1} term in the k_j^{n+1} solution, a comparison was made between the algebraic result of solving the equations directly, and a replacement of η_j^{n+1} with η_j^n as might be expected for an equation in conservative form that the normal Lax-Friedrichs method requires. With no initial velocity and the initial Gaussian water height, there was no difference between η_j^{n+1} and η_j^n as the wave propagated. However with the under-toe initial conditions that results in a near-break situation, the η_j^n substitution did not result in a stable solution beyond 450 steps, as shown in Fig. 1.8 comparing the two at 485 steps, just before a portion of the wave reaches a vertical line with slope ∞. This resulted in a numerical instability in the model but suggests even more strongly that the wave would have broke if multiple-valued solutions were allowed.

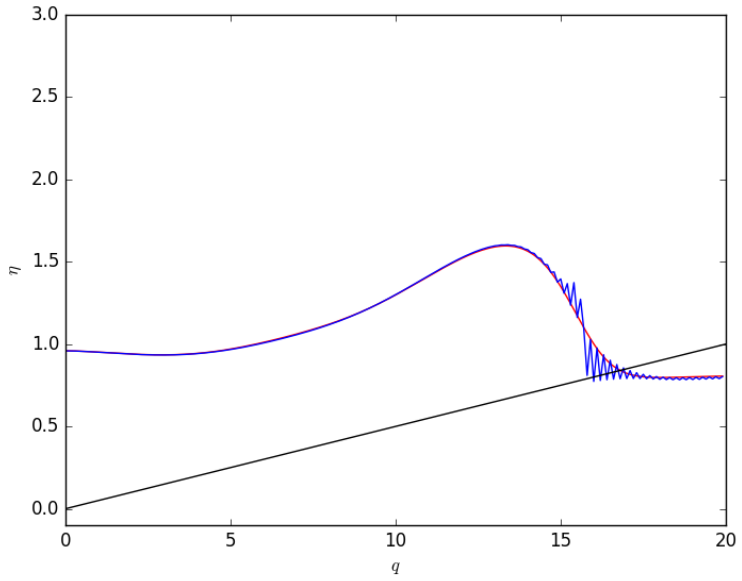

Figure 1.8: Comparison of the stability of η_j^{n+1} in the k_j^{n+1} equation. The calculated solution including η_j^{n+1} is the smooth function, while the modified version substituting η_j^n is the more jagged solution with discontinuities beginning to form. This modification resulted in instability and is shown at 485 steps, just before the discontinuities grow to infinity and the model breaks.

Chapter 2

Balls and Springs

In the previous chapter, waves were unable to break due to the numerical model that required a single-valued solution. In this chapter, a simpler physical model is used that does not prevent a multiple-valued solution: considering the surface of the water as a line of balls connected by springs, ignoring the behavior of the bulk of the water beneath the surface. The acceleration of a single ball in this system is only impacted by the behavior of those directly adjacent, so there is nothing in the model that prevents a multiple-valued solution. This results in a system in which, if set up correctly, a wave could break and spill over. However, it's worth noting that the physical usefulness of this model is inherently limited. Since the interactions between the balls are only governed by the separation of adjacent balls, the surface of the water in this model could pass through itself without any change in behavior, at which point this simulation can no longer be considered physically relevant. Loops in the break are also possible, and this is not a physically meaningful result, but can be interpreted as the point at which energy in the system would dissipate through turbulence if the model allowed for such complex behavior.

For a short time, despite these drawbacks, this model can produce the desired result and provide useful insight into the behavior of the wave break without the extreme computational expense. Despite the limited circumstances in which this model might seem to apply, its purpose is to further the methods of the previous chapter to get a wave to break eventually. Chapter 3 will focus on the combination of these models, which will use the methods of Chapter 1 to set up a wave based on the (approximate) physics of water, which is passed into this ball and spring model to view the wave break. Therefore in this chapter, the physics of water is set aside in part, since the relevant physics will be mostly present in the precise initial conditions used to start the model, with changes made by modification of the spring constant based on physically relevant parameters of the wave, namely wave height and water depth. The main components of a ball and spring system are the spring constants k between each ball, each of which has a mass m.

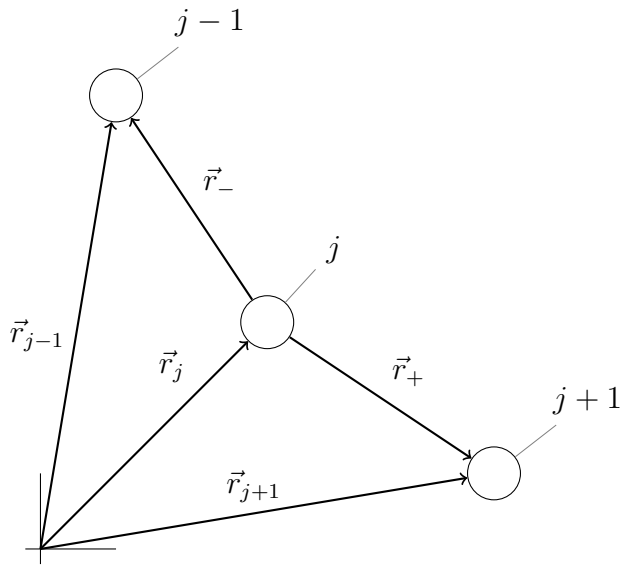

Figure 2.1: Setup for the ball and spring model.

2.1 Elastic Network Models

Simple models similar to this connected line of springs, despite appearing disconnected from the relevant physics of the problem, are actually frequently used in molecular dynamics. Representing each particle as a ball, and then connecting each one to all the others via springs, the complex behavior of molecules and proteins can be modeled to close accuracy. The behavior of each spring is modified to account for all of the relevant forces to a molecule, including atomic bonds, Van der Waals forces, electromagnetic forces, and more. In the case of water, the spring is collecting all of the relevant physics including pressure, surface tension, viscosity, and the Navier-Stokes equations for mass, momentum, and energy conservation. Examples of this method used in biology can be found in [6], and for molecular research in [7]. While it might seem absurd that this method could yield some useful results, note that a single line of these springs, without the complex network of connections used in biology and chemistry, is like a string, and is capable of simple wave-like behavior (see Fig. 2.2). A small injection of physics by modification of the spring constant will give it more complex wave-like behavior.

2.2 Equations

Consider a connected line of springs, forming a path between two end points. The balls connecting the springs together model the particles of water, and the springs model all of the relevant physics. To derive the acceleration for each ball in this system, consider three balls in two dimensions, connected with two springs, shown in Fig. 2.1. The center ball will be indexed j, referring to the current ball whose

acceleration is being calculated, and since each ball only has two neighbors, the state of the rest of the larger system does not contribute within a single time step. The endpoints will be fixed, so each ball that can move will be governed by these equations.

Ball j has two neighbors, indexed $j-1$ and $j+1$, based on their ordering if they were in a straight line between the endpoints. This is so the position of each ball can be placed into a list, where indices $j-1$ and $j+1$ in the list will always refer to balls that are connected. In so doing, the connections between the balls cannot be changed, creating the issue of what happens when one part of the line crosses through another. In the most realistic simulation, the connections between balls would be changing at each step in time to ensure a physically interpretable solution at all times. This is essentially what is done in a highly realistic method called smoothed particle hydrodynamics, but is done at a considerable computational expense. I dodge the issue here by simply stopping the simulation when the line of springs crosses over itself, noting that another physical process must be taking place that is not considered here, and an algorithm that varied the connections would prevent this from forming.

The position of a ball in space is defined by a vector from the origin, $\vec{r}_j$, and vectors pointing from ball j to its neighbors are defined such that

$$\begin{aligned} \vec{r}_+ &= \vec{r}_{j+1} - \vec{r}_j \\ \vec{r}_- &= \vec{r}_{j-1} - \vec{r}_j. \end{aligned} \tag{2.1}$$

Force for a spring is given by Hooke's Law,

$$F = k(r-a), \tag{2.2}$$

where r is the total length of the spring, the separation between the two balls, and a is the unstretched length of the spring, so $r = a$ results in no force. Adding the two forces for each of the two springs attached to a ball using Eq. 2.2, the total force on ball j is given by

$$\vec{F} = k(|\vec{r}_+| - a)\hat{r}_+ + k(|\vec{r}_-| - a)\hat{r}_-, \tag{2.3}$$

where $\hat{r}$ denotes the unit vector in the direction of $\vec{r}$ pointing outwards as shown in Fig. 2.1. To maximize the water-like behavior of the system, the endpoints were fixed in position by setting their mass to infinity, which prevents the whole system from moving in a single direction. This boundary condition helps to simulate the presence of water with no net velocity on both sides of the region from 0 to L. Initial conditions were specified using a function calculated at points equally spaced in the horizontal direction. This method of specifying initial conditions does not make the spacing, $\vec{r}_+$ and $\vec{r}_-$, equal in length across the whole system. Instead, there is some initial tension upwards or downwards, just based on the initial height above or below the endpoints. In its initial state, regions of the system above the endpoints will have an initial net downward force, and regions below would have a net upward force. This introduces an analog to gravity and pressure that is not easily handled by adding explicit forces to each ball. For example, adding a downward acceleration to each ball would cause the whole chain to fall, resulting in a simulation not of a wave but of a hanging string,

like an electric line between two poles. Adding upward pressure explicitly to each ball would also be rather challenging since such an equation would rely at least in part on the depth of the water at that point. The overhanging edge of the breaking wave should have less upward pressure than a region supported by a column of water all the way to the bottom. But without specifying any physics directly, the model will have the qualitatively correct behavior for a wave.

2.3 Verlet

One of the most common methods for integrating Newton's second law in this case is the Verlet method [8], which again makes clever use of Taylor expansion. The method is time reversible, meaning that energy is implicitly conserved. Using a temporal spacing of Δt, if the position at an initial time t is known, then the time at $t + \Delta t$ and $t - \Delta t$ can be separately calculated using a Taylor expansion, [9]

$$\begin{aligned} x(t + \Delta t) &= x(t) + v(t)\Delta t + \frac{1}{2}a(t)\Delta t^2 + \mathcal{O}(\Delta t^3) \\ x(t - \Delta t) &= x(t) - v(t)\Delta t + \frac{1}{2}a(t)\Delta t^2 + \mathcal{O}(\Delta t^3). \end{aligned} \tag{2.4}$$

Velocity and acceleration are defined by their derivatives as usual, $v(t) = \frac{\mathrm{d}x}{\mathrm{d}t}$ and $a(t) = \frac{\mathrm{d}^2x}{\mathrm{d}t^2}$. The Taylor expansion is an infinite sum, and higher order terms contribute less and less to the result, so higher order terms can be dropped. In this application, only terms up to second order are needed for an accurate solution. The two equations are then added to eliminate the velocity term, giving

$$x(t + \Delta t) \approx 2x(t) - x(t - \Delta t) + a(t)\Delta t^2. \tag{2.5}$$

With this method, only the positions of balls at time t and $t - \Delta t$ are needed to propagate the solution forward in time, given $a(t)$ as defined in Eq. 2.3. This equation is easily time reversible, solving instead for $t - \Delta t$,

$$x(t - \Delta t) \approx 2x(t) - x(t + \Delta t) + a(t)\Delta t^2 \tag{2.6}$$

a unique property of the Verlet method. Since velocity was explicit in the previous chapter, to ensure that the data can be interchangeable and plugged into this model, a modification in the first time step is necessary to accommodate an initial velocity as opposed to multiple initial positions. This can be done by omitting the addition of the two equations in Eq. 2.4, simply taking

$$x(t + \Delta t) \approx x(t) + v(t)\Delta t + \frac{1}{2}a(t)\Delta t^2, \tag{2.7}$$

and continuing with Eq. 2.5 for all future times.

2.4 Constant k

With a constant value of k for all points, the system behaves like an elastic string. Given an initial Gaussian, the peak collapses, resulting in two waves traveling to either side, similar to the behavior of a water wave, except that the wave then wraps around the fixed endpoints, and moves backward and upside down with the same behavior, shown in Fig. 2.2. This isn't the most water-like behavior, so some changes need to be made. First, a damping force can be applied in the form

$$F = -\gamma m v, \tag{2.8}$$

such that

$$a(t + \Delta t) = a(t) - \gamma \cdot v(t + \Delta t), \tag{2.9}$$

where γ is a small constant. This value was chosen to be 0.1, which still allows the wave to propagate, but not significantly decrease in height as it moves across the simulation window a single time. Times at which the wave wraps around the endpoints should be ignored since they cannot be physically accurate. To make the ball and spring model physically compatible with the previous chapter, a wave with the same initial conditions should travel at a dimensionless speed of 1. k was set so that the highest point of the wave travels at a speed of 1, resulting in a dimensionless k value of 24.

2.5 Changing k by angle

As is expected in the behavior of a non-linear string, k can be modified based on the curvature of the string. For a discrete system, the angle between the adjacent points will be used to set the spring constants. Shown in Fig. 2.3, k for the spring between balls $j - 1$ and j is determined by the angle θ,

$$k = k_2(1 - \frac{\theta}{\pi}) + k_1. \tag{2.10}$$

With this equation, the spring constant will vary between k_1 and $k_2 + k_1$, and the points with the highest curvature will have k closer to the maximum. A wave close to breaking appears to have the maximum curvature close to the leading edge of the wave, and with this method of determining k, if the springs are under tension, they should be pulled together more in this region and cause some of the balls to be forced forward in the direction the wave is traveling. This is an improvement, as the wave steepens at some points, but it does not spill over, and the system resists the tendency to develop a double valued solution. Due to the way in which angles are measured, this method also can lead to instabilities, as tiny deviations between points close together can result in large calculated angles even when the larger system appears mostly flat. This eventually leads to a much larger or smaller k than adjacent points, and the solution can quickly diverge.

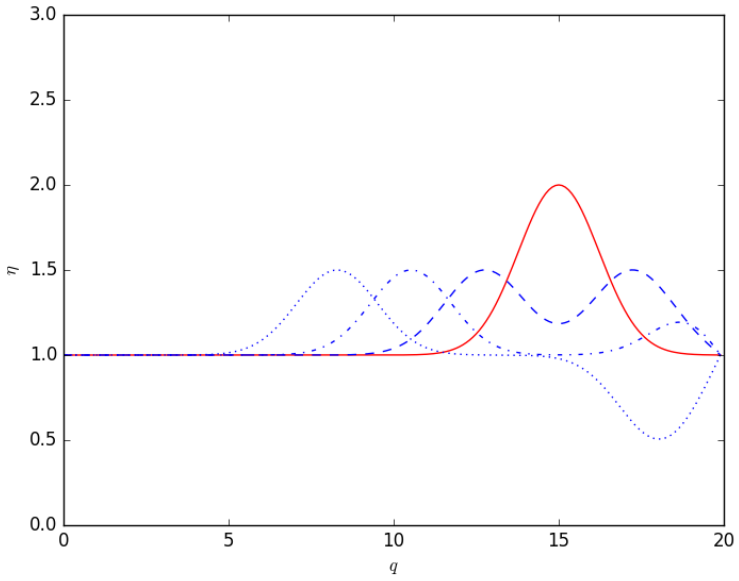

Figure 2.2: Basic behavior of a connected spring system with fixed endpoints. The initial Gaussian wave collapses in the center and creates two waves that propagate to the left and right. The wave height decreases and is reversed as it moves past the endpoints, and the wave then propagates the other direction but upside down. The initial height is a solid line, with the dashed lines at later times.

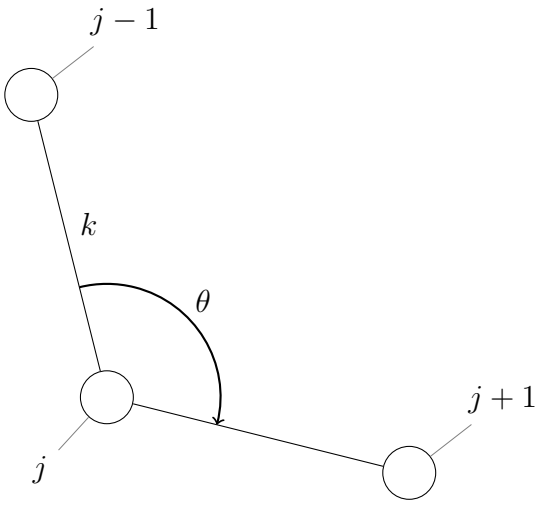

Figure 2.3: Description of angles used to modify k. This is similar to the curvature of a string adapted from a continuous to discrete system.

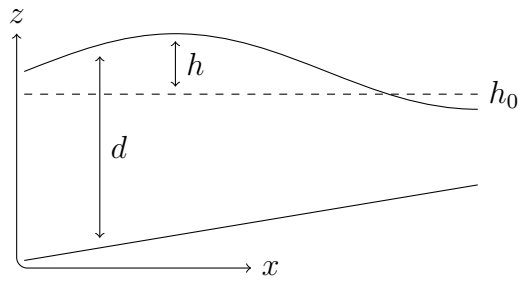

Figure 2.4: Relevant variables used in Eq. 2.11. h is the height of the wave above the ambient water height, h_0, and d is the depth of the water at that point, the distance to the linear sloping bottom.

2.6 More physical k

In an attempt to develop an equation that sets k based on the physics of the sloped bottom water wave, k can be a function of the depth of the water d and the height h above the calm water level h_0, shown in Fig. 2.4. For a wave near-breaking, the velocity of the water is similar to Fig. 2.8. To mimic this velocity profile, the highest points on a wave should have the highest k, and these values should increase as the wave approaches the shallower water,

$$k = k_1 + \left|\frac{h}{d}\right| k_2. \tag{2.11}$$

With this equation, a wave break is possible! For an initial Gaussian wave height, the initial velocity was set as a Gaussian, centered with the initial wave so that the entire Gaussian is moving to the right. With an initial peak velocity above 1, the wave can break. With this k update function, the wave spills over and becomes a double valued solution. However, since the balls can pass through each other, it cannot provide information about the water behavior as the leading edge of the breaking wave passes through into the water. Furthermore, as the wave moves after breaking, the leading edge forms a loop, that then dominates the wave behavior and leaves just a propagating loop, shown in Fig. 2.5. This is not a physical behavior but indicates that there are some details not included in the model, like turbulence or the change in the way gravity affects the overhanging region to account for the change in energy.

2.7 Energy measurement

The energy in each ball can be calculated by

$$E = \frac{1}{2}mv^2 + \frac{1}{2}k(r-a)^2. \tag{2.12}$$

These energies are then categorized into small bins by x position, and each bin is averaged, creating a plot of $E(x)$, shown in Fig. 2.6. Areas where the springs are most

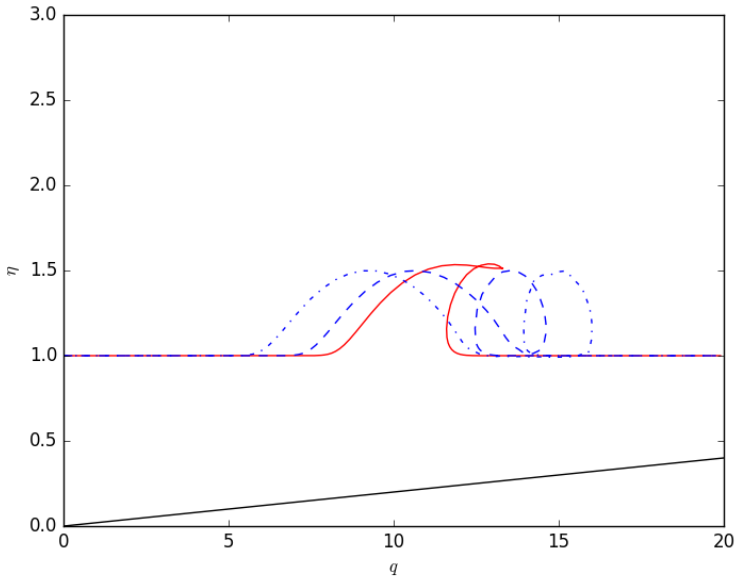

Figure 2.5: With the damping term $\gamma = 0$, the loop that initially forms to break the wave increases in size until the wave is only represented by that loop propagating to the right. Each dashed line further to the right represents a later point in time.

stretched, compressed, or high up have the greatest energy, which corresponds to just behind the peak of the wave. Since the wave is moving to the right, it compresses the springs ahead of it and stretches the ones behind.

2.8 Energy k

To further the accuracy of the height and depth based modification of k, consider the potential energy of a spring,

$$E = \frac{1}{2}k(r_- - a)^2, \tag{2.13}$$

where r_- is the length of the vector $\vec{r}_-$. Setting this value proportional to the height with a constant c,

$$\frac{1}{2}k(r_- - a)^2 = ch \tag{2.14}$$

or

$$k = k_1 + \frac{2h}{(r_- - a)^2}k_2, \tag{2.15}$$

where k_1 and k_2 are chosen to limit the possible range of k. To make this more similar to the previous section, note that while wave energy is concentrated near the surface, some energy is stored at a depth considerably greater than those used in the simulations, since the motion of the water in a passing wave influences the water around and below it. As the water decreases in depth, this energy must go

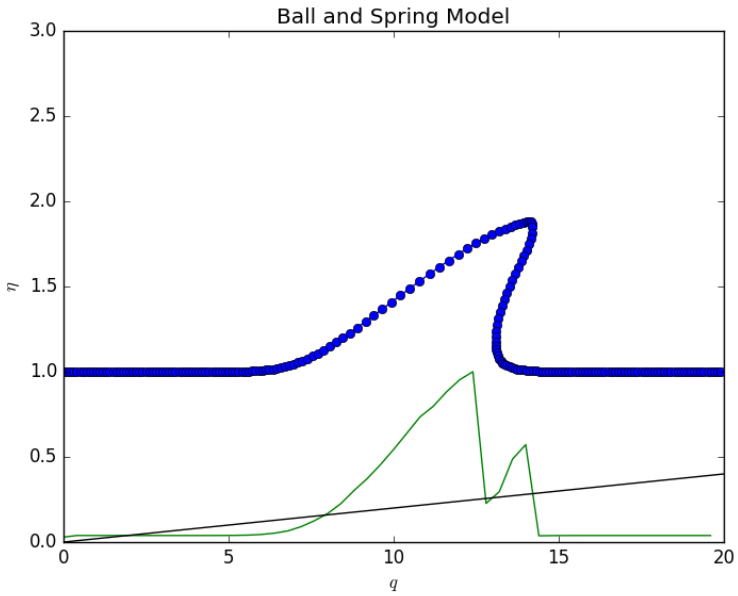

Figure 2.6: Energy for a wave using the update for k in Eq. 2.15, shown in the lower line with the wave above. Energy peaks just behind the peak of the wave, where the springs are the most stretched. But more importantly, a second peak is visible at the leading tip of the wave, which corresponds to a region in which the springs are compressed, and the modified spring constants give that region a boost in energy.

somewhere, and it moves upward and causes it to increase in height. This eventually causes the wave to break. We can introduce a term analogous to this behavior, where the energy contained in the surface increases with decreasing depth. In this way, energy is not explicitly conserved, but keep in mind that any energy change underwater was previously ignored by this model (and to some extent the previous one as well). If this model is working correctly as an accurate representation of reality, the critical velocity at which the wave breaks should decrease as the depth increases, since a wave traveling at a constant speed should, at some depth, not break, and then at a shallower depth closer to the shore, break. This ignores the backward flow from the previous wave that would assist the break on a real beach. This situation is analogous to a tsunami where the approaching wave has a velocity large enough that the receding water does not affect the way the wave breaks. This is a reasonable analogy because the assumptions made in the linearized shallow water equations are most accurate for tsunamis than regular ocean wind waves, and its predicted velocity relationship is met with this method.

2.9 Breaking Test

To investigate whether or not the ball and spring model is capable of producing a wave break, the initial conditions for both position and velocity were tweaked until the desired qualitative behavior was found. This was

$$\begin{aligned} x_0 &= e^{-2(x-c)^2} + 1 \\ v_0 &= v_p e^{-2(x-c)^2}, \end{aligned} \tag{2.16}$$

where v_p is the chosen maximum of the Gaussian, and c is the position at which the wave is centered. With these initial conditions, the initial Gaussian is pulled to the right with its initial velocity, and if the velocity is greater than 1, the wave moves far enough to the right before falling, giving the desired behavior for wave breaking, before a loop forms in the leading edge that grows in size. If the velocity is initially too low, the wave does not break, but instead a loop forms that travels to the right, while a small wave travels to the right. The desired behavior for a large initial velocity is shown in Fig. 2.7. To ensure that this is a realistic condition for a water wave, note the velocity profile for the right traveling wave in a fluid, calculated in Chapter 1. This is shown in Fig. 2.8, and contains components for both a right and left traveling wave. Considering the right traveling wave only, this shape is reasonably approximated by a Gaussian, especially the parts further to the right at the leading edge where the wave breaking is taking place.

Now that the wave breaks as is desired, based on conditions similar to those found in Chapter 1, the two methods can be combined to ensure the most realistic initial conditions possible for the ball and spring model.

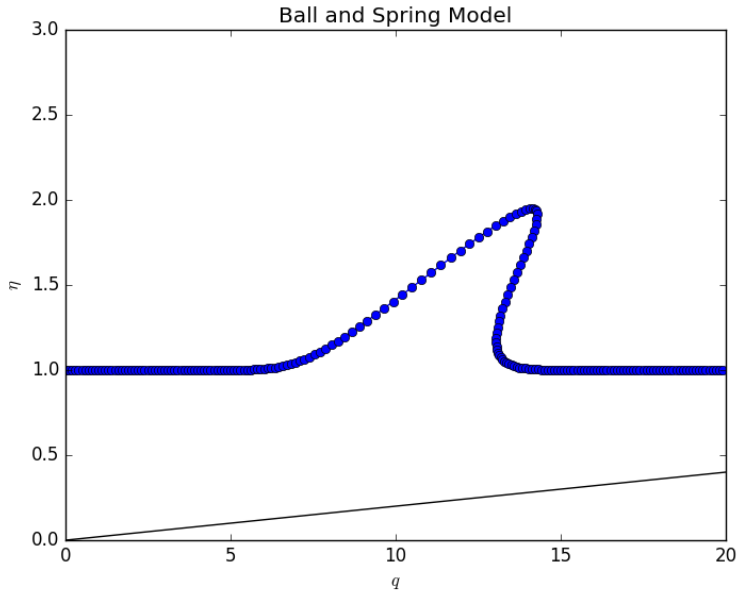

Figure 2.7: Wave breaking, with initial wave velocity to the right.

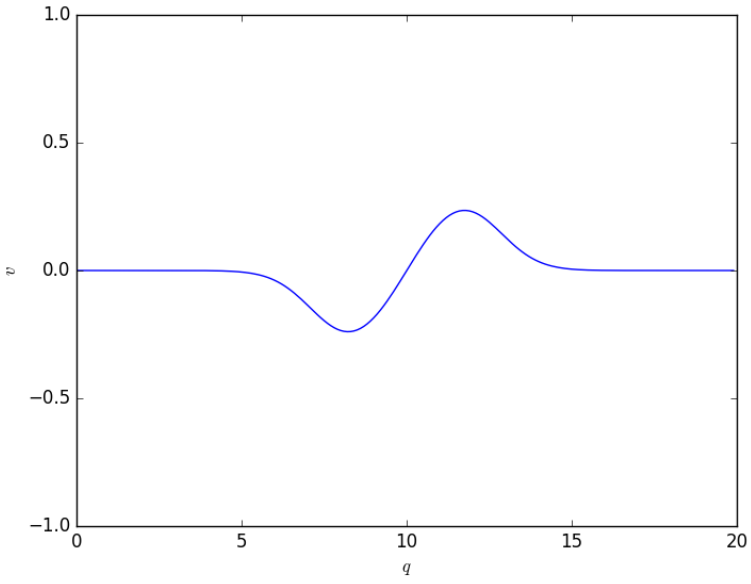

Figure 2.8: Velocity profile given by the methods in Chapter 1 for a collapsing Gaussian, shortly after the simulation begins. The velocity profile for the right and left traveling waves is each close to a Gaussian, so using that as the initial velocity of the ball and spring model is reasonable.

Chapter 3

Combination of Methods

The combination of these two models will create a simulation that closely follows the physics of actual water in the beginning, and then transitions the state of the wave into a more simple model that can allow the wave to break.

Let's quickly review where we're at. Chapter 1 used the actual physics of water waves, using a modification of the shallow water equations. With realistic initial conditions chosen for this model, the wave will develop a height and velocity profile over time that will closely match a natural wave approaching a beach. As the depth of the water decreases, the wave increases in height and the wavefront steepens. At this point, the Lax-Friedrichs model is no longer accurate. It cannot give multiple-valued solutions, and the vertical and horizontal components of velocity are coupled so that this will not occur. The ball and spring model is a suitable solution to this problem, and it is perfectly capable of producing complex multiple valued solutions. We found in the previous chapter that the ball and spring model is capable of producing a wave that has the correct qualitative behavior, and a rough comparison showed that those specific initial conditions are somewhat similar. Now is the time to see if the combination of these two models will produce an accurate simulation of a breaking wave.

3.1 Conversion of Data

The Lax-Friedrichs model discretizes space into regions that are fixed in space, and have the height and velocity of the wave calculated at each of those points. The ball and spring model uses a very different method of defining the wave, with moving calculation points that only have their position defined. Conversion of data between these models is non-trivial and requires some special attention. Velocity using the Verlet method is calculated by comparing the position of a ball at two points in time,

$$v(x,z) = \left(\frac{x_n - x_{n-1}}{\Delta t}, \frac{z_n - z_{n-1}}{\Delta t} \right), \tag{3.1}$$

where n is the current time step. This method could be applied to the velocity calculation using the last two data points from the Lax-Friedrichs method. But if the

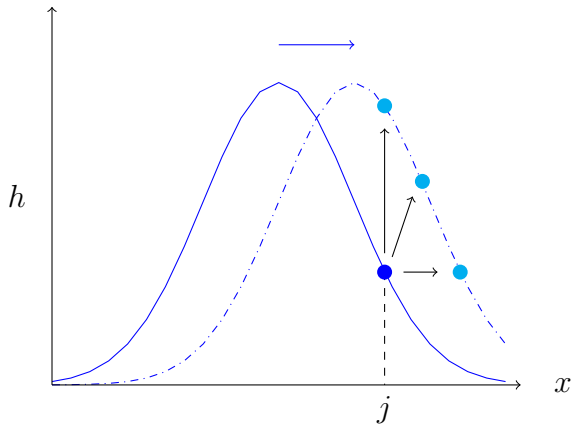

Figure 3.1: Assuming the initial position of the ball is at the height of the wave for calculation point j, I could assume that the ball in the next time step had moved to any of the other points (or more) shown for a wave moving to the right. If the point were to move directly up, the vertical component of velocity would change significantly between the two models, but if it only moves to the right, it neglects some non-zero vertical component.

wave is moving, the question of where a single ball is moving from one time to the next is unclear. It might be reasonable to assume that each ball is moving horizontally with the wave, but assuming that each ball moves *only* horizontally between time steps neglects the vertical component of velocity, which is clearly non-zero since we observed the collapse of waves in Chapter 1. However, measuring this vertical component cannot be done in the same way that the horizontal component was measured since a subtraction would suggest a much higher vertical velocity (up ahead of the wave, and down behind it) than is present. Now, this vertical component of velocity appears to conflict with Eq. 1.6, where we required that the vertical component of the velocity be zero. This boundary condition, however, restricts the flow of water through the top surface and does not prevent the surface itself from moving up and down.

Since the simulation is using the shallow water wave equations, the general behavior of the wave is similar, despite the modifications that were made to account for the change in the depth. This suggests that $v_z \ll v_x$, and it's okay to ignore this component and set v_z to zero. But by neglecting this component, there are cases in which the leading edge of the wave appears to stop in the shift between models, and the back part of the wave simply collapses over it. To counteract this, I applied a uniform constant velocity in addition to the Gaussian over the initial wave, which forces $v_z \ll v_x$ even more strongly than before, and the result is a much smoother transition between models. Another potential solution could be to track the position of the wave using a fitline, and try to guess how it could be translated to the right or left to where the wave is at another time, but as the wave approaches shallower water we expect that shape to change, and I chose to avoid making assumptions about which parts of the wave would remain unchanged.

3.2 Parameters for the Full Simulation

The model was setup with an initial Gaussian of height 1 above the mean water level of 1,

$$\eta_0(q) = e^{-\frac{1}{2}(q-5)^2} + 1. \tag{3.2}$$

Slope α was set to 0.02, the same as used in [10]. The initial $k = hv$ (from Chapter 1), encoding the velocity of the wave, was set to 1 to give the entire system some initial velocity and the peak velocity of the wave was set to 3.5, with a Gaussian of the same width as the height,

$$k_0(q) = 3.5e^{-\frac{1}{2}(q-5)^2} + 1. \tag{3.3}$$

As before the window from $L = 0$ to $L = 20$ was divided into 200 calculation points with space and time steps

$$\begin{aligned} dq &= \frac{L}{200} \\ ds &= \frac{dq}{10}. \end{aligned} \tag{3.4}$$

The Lax-Friedrichs model was run for 100 steps, up to a non-dimensional time $s = 1$. The data was then converted into positions for individual balls and springs, assuming all velocity is horizontal. The lowest value of the spring constant k was set to 2.4, which was chosen to ensure that the waves with an initial velocity traveled at the same speed in both models. The spring constant was varied according to Eq. 2.15, with $k_2 = 2.4$ so that the spring constant could at most double. The equilibrium distance for the springs was set with some initial tension,

$$a_0 = \frac{L/n}{5}, \tag{3.5}$$

where n is the number of balls in the system, taken to be the same as the calculation points in the Lax-Friedrichs model. The time step ds was the same, and the initial horizontal spacing of balls was set using dq, so that each ball started at the same point as the calculation points in the first model. The damping term γ was set to 0.1. The Verlet model was run until a loop formed in the tip of the breaking wave.

3.3 Results

The initial state of the wave defined by the two Gaussian functions for height and velocity start the simulation as shown in Fig 3.2 at time $s = 0$, where all of the water is moving to the right with initial velocity. The Lax-Friedrichs model ran for 100 steps and the final frame in that model is shown at $s = 1$. This, and the frame before it determine the initial state of the ball and spring model. As soon as the ball and spring model begins, the wave begins to move towards breaking, since there is nothing preventing the wave from having a multiple valued solution, and the top of the wave is moving faster than the bottom. The wave at $s = 2$ is shown 100

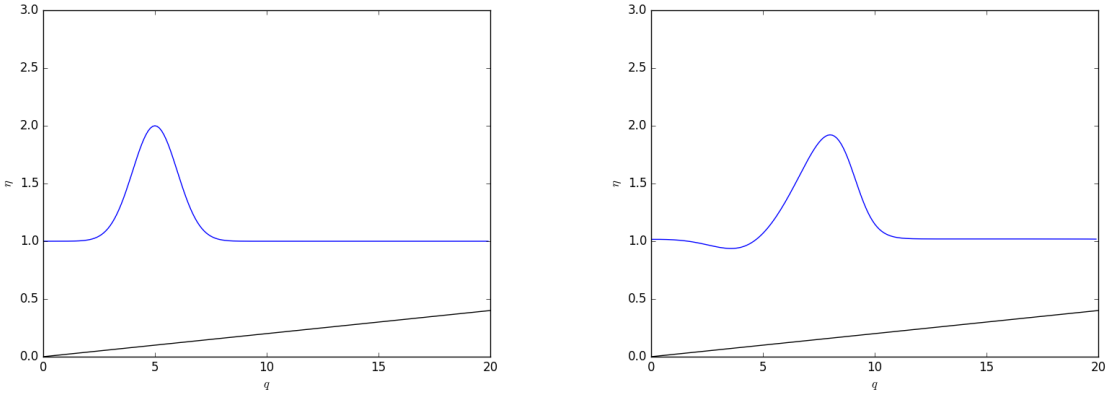

$s = 0$

$s = 1$

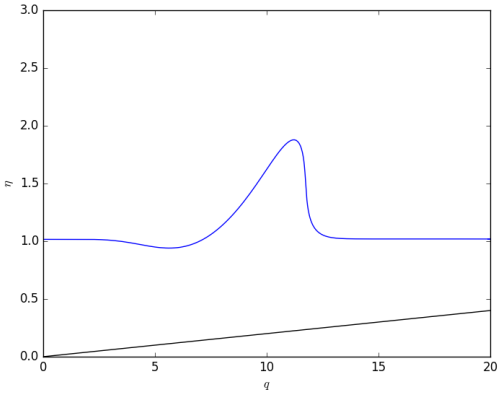

$s = 2$

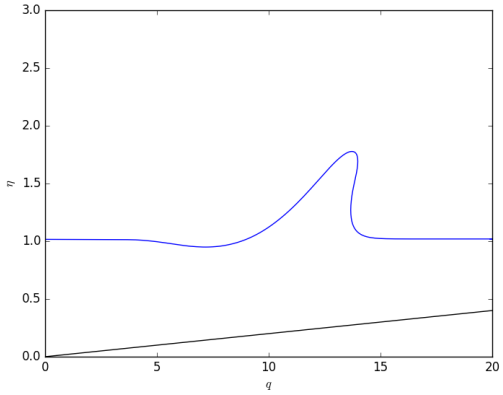

$s = 3$

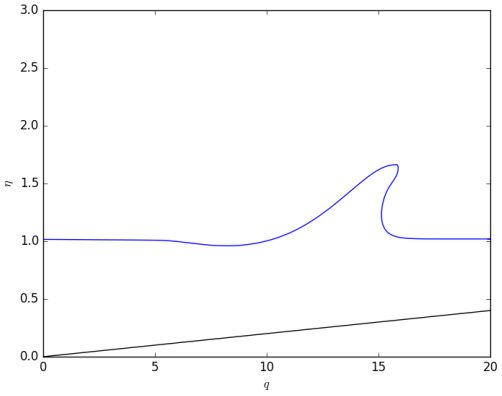

$s = 4$

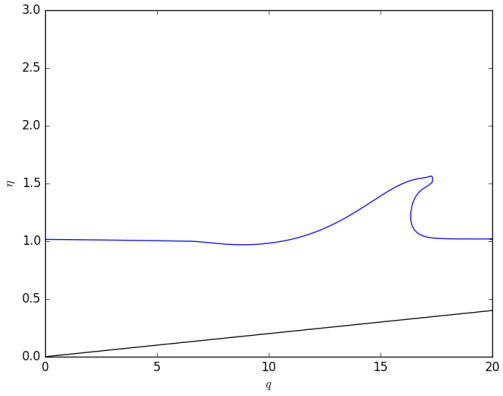

$s = 5$

Figure 3.2: The full simulation shown from $s = 0$ to $s = 5$. The Lax-Friedrichs model runs from 0 to 1, and the Verlet model runs from 1 to 5.

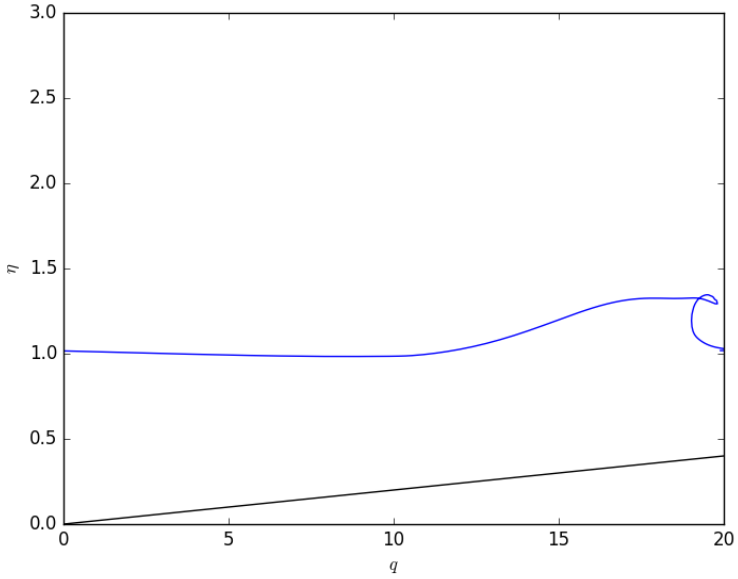

Figure 3.3: Wave at $s = 8$. The leading edge of the wave collapses and forms a loop, at which point the solution is no longer an accurate representation of wave behavior.

steps into the ball and spring simulation. It's clear that the wave immediately tends towards breaking within the ball and spring model. By the time the wave reaches $s = 3$ the ball and spring model has been running for a total time of $s = 2$, and the wave has developed a multiple valued solution, which defines breaking. This is about the moment at which the ratio h/d can be measured, which is a useful non-dimensional way to compare this simulation to experiments performed on real ocean waves or in wave tanks. The breaking portion of the wave continues to develop at $s = 4$ and $s = 5$, where the overhanging edge begins to fall, which is exactly the desired behavior for a wave in real life, as gravity would dominate this region that is not supported by water underneath. The evolution of the wave from $s = 1$ to $s = 7$ is shown combined for comparison in Fig. 3.4. By time $s = 8$, a loop forms, shown in Fig. 3.3, and the solution is no longer physical. At times beyond this, the loop grows in size and the wave collapses until it is just the loop traveling to the right. Damping helps to reduce the size of the loop, but solutions containing it must be ignored until further research is done on what exactly it means to turn water inside out on itself. Eventually, the leading edge of the wave crosses over itself and forms a loop, at which point the simulation can no longer be considered physical. I imagine inside this loop being the region that becomes unstable within the wave and plunges straight down due to gravity, which I did not explicitly include in the model, although it was implicitly considered in the changing of the spring constant. This could also be a turbulent region where white-water forms on the top as you might see in a large wave breaking on a beach.

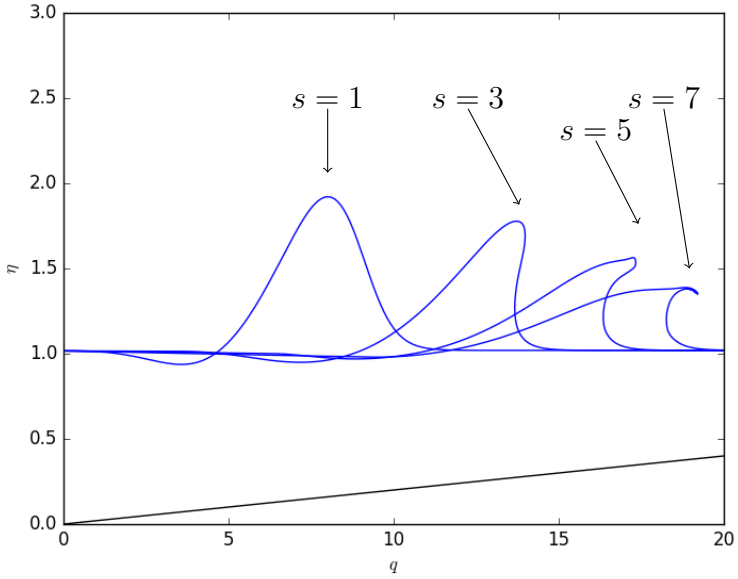

Figure 3.4: Full simulation of the wave.

3.4 Comparison to Experiments

With the desired qualitative behavior achieved, it's useful to look at how the dimensionless height and velocity compare to experimental data. There have been many experiments, both done in wave tanks in the lab and the field, studying the behavior of breaking waves on beaches.

Linear Airy wave theory has been used for predicting the breaking behavior of a wave based only on its characteristics offshore, where the depth does not influence its behavior. Komar and Gaughan [11], using this theory, predict that the breaking height should be

$$h_b = cg^{1/5}(TH_\infty^2)^{2/5}, \tag{3.6}$$

where c is some constant, T is the wave period of the wave train, and H_∞ is the height of the wave in deep water. Waves don't (often) exist in isolation in the real world, so my simulation of a single wave must be considered as part of a very large number of similar waves traveling together. The constant c is determined experimentally and was found to be $c = 0.39$ in a study by Weishar and Byrne [10]. Also, to account for a difference between the experimental results of Weishar and Byrne and my own, a factor of 0.92 adjusts this prediction in the case where the region in front of the wave does not decrease in height, giving $c = 0.359$. With this, the only additional values needed to find the breaking height are T and H_∞. At $x = 0$, the water is at its deepest point, so we could define this to be "deep" here. Given an initial Gaussian with height one above the mean water level, we can then say that $H_\infty = 1$. A reasonable value for T can be found from forecast data, for surfing areas or from offshore buoys. I found that a period of 10s was predicted on April 5$^{\text{th}}$, 2017 and is

common on the Oregon coast [12]. Given these conditions, h_b is expected to be 1.76 meters. Now to convert these non-dimensional results into dimensional quantities to compare to an experiment, we'll use the equations that helped to remove all of the dimensional quantities for the equations of motion in Chapter 1,

$$\frac{h_0}{t_0} = v_0 \quad x_0 = h_0 \quad t_0^2 = \frac{h_0}{g}. \tag{3.7}$$

Choosing $h_0 = x_0 = 1$ m,

$$t_0 = \sqrt{\frac{h_0}{g}} = 0.32\,\text{s}, \tag{3.8}$$

$$v_0 = \sqrt{gh_0} = 3.13\,\text{m/s}. \tag{3.9}$$

The non-dimensional results for breaking height and velocity were

$$\eta_b = 0.86 \quad \frac{k_b}{\eta_b} = 1.35, \tag{3.10}$$

so,

$$h_b = 0.86\text{m} \quad v_b = 4.23\,\text{m/s}. \tag{3.11}$$

The breaking velocity v_b for water of depth less than one meter can be calculated according to the the experiment performed by Siefert [13], which suggests

$$v_b = g(d + 0.75h_b), \tag{3.12}$$

which predicts the breaking velocity should be 13.58 m/s. Another useful comparison is to calculate the ratio h/d at the breaking point, where the velocity of the wave is at its minimum for breaking to occur. The maximum height at breaking was 0.86, which was at a depth of 0.74, for a total distance from surface to bottom of 1.6, so

$$\frac{h}{d} = \frac{0.86}{0.86 + 0.74} = 0.54. \tag{3.13}$$

Komar and Gaugan predict this value to be 0.7, and the experiment by Weishar and Byrne suggests a value of 0.86.

Overall, these results are mostly within the same order of magnitude, and given the numerous assumptions and simplifications made to the physical behavior of the wave throughout, these results suggest that my simulation is quite close to a model for a breaking wave on a beach in some specific cases.

Conclusion

Waves are incredibly complex non-linear phenomena that physicists have struggled to model accurately, even in the age of the supercomputer. Instead of considering every detail of the behavior of water to get a wave to break exactly how it would in the real world, I used the minimum required to get a wave to break with the same basic behavior. I created a model based on the Navier-Stokes equations, that when used in the Lax-Friedrichs finite difference numerical method create a reasonably realistic simulation that can model wave behavior in most conditions. I also created a ball and spring model, used in molecular dynamics simulations to remove some of the important physics and allow the solution for the height of the wave to take on multiple values at a single point. Combining these, I created a Frankenstein numerical method that took advantage of simpler solutions for both the single valued and multiple valued regimes. The results from the full simulation of the wave breaking are similar to experiments done in both wave tanks and at beaches, and some parameters like the non dimensional height-to-depth ratio at the breaking point were spot on with both theoretical and experimental oceanographic research.

All of the code for this thesis was written in Python, taking advantage of the packages NumPy and SciPy, as well as MatPlotLib for the creation of animations and figures. All of the code is available at `http://people.reed.edu/~jfrankli/senior.theses/files/Freymiller.zip`.

References

[1] J. H. Ferziger and M. Peric, *Computational Methods for Fluid Dynamics*, Springer, 1999.

[2] J. Franklin, *Computational Methods for Physics*, Cambridge, 2013.

[3] M. B. Liu and G. R. Liu, Archives of Computational Methods in Engineering **17** (2010).

[4] L. Howard, *A Numerical Investigation of Water Waves*, Reed College, 2013.

[5] L. Milne-Thomson, *Theoretical Hydrodynamics*, Dover, 1996.

[6] D. H. Boal, *Mechanics of the Cell*, Cambridge, 2002.

[7] J. Franklin, P. Koehl, S. Doniach, and M. Delarue, Nucleic Acids Research **35**, W477 (2007).

[8] L. Verlet, Phys. Rev. **159**, 98 (1967).

[9] M. P. Allen and D. J. Tildesley, *Computer Simulation of Liquids*, Oxford Science, 1989.

[10] L. L. Weishar and R. J. Byrne, Field study of breaking wave characteristics, in *Proceedings of 16th Conference on Coastal Engineering*, 1978.

[11] P. D. Komar and M. K. Gaughan, Airy wave theory and breaker height prediction, in *Proceedings of 13th Conference on Coastal Engineering*, 1972.

[12] NOAA national data buoy center, http://www.ndbc.noaa.gov/.

[13] W. Siefert, Shallow water wave characteristics, in *Proceedings of 13th Conference on Coastal Engineering*, 1972.